Electronic Supplementary Material (ESI) for ChemComm.
This journal is © The Royal Society of Chemistry 2016

Supporting information

In operando observation of sodium ion diffusion in a layered sodium transition metal oxide cathode material, P2 $Na_xCo_{0.7}Mn_{0.3}O_2$

Steinar Birgisson[a], Yanbin Shen[b] and Bo B. Iversen*[a]

[a]Center for Materials Crystallography, Department of Chemistry and iNANO, Aarhus University, DK-8000 Aarhus C, Denmark

[b]Synfuels China Technology Co. Ltd., Leyuan South Street II, No.1, Yanqi Economic Development Zone C#, Huairou District, Beijing, 101407, China.

*bo@chem.au.dk

Contents

P2 crystal structure 2
Normalized scale factor 2
High potential phase transformation 3
Experimental section 4
Synthesis 4
Characterization 4
Rietveld refinements of pristine material 4
In operando data collection 6
In operando data analysis 7
Notes about sequentially refined sodium occupancies 7
Elemental composition 8
High Resolution Transmission Electron Microscopy coupled with Energy Dispersive Spectroscopy 8
References 9

P2 crystal structure

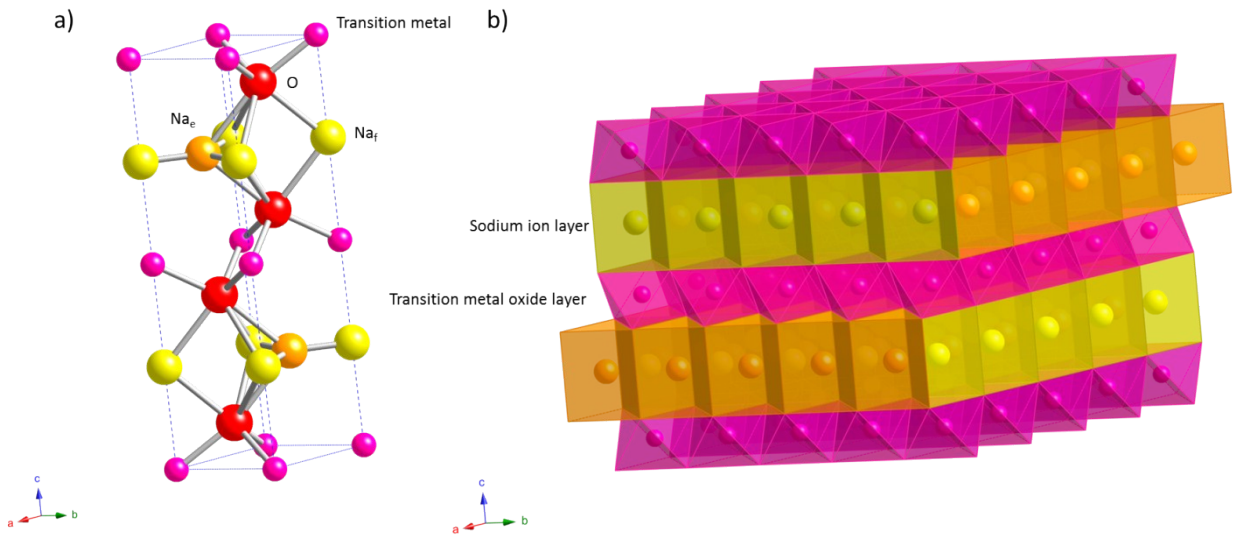

Figure S1. a) Atomic positions in the unit cell of the hexagonal P2 phase b) Extended structure of the P2 phase showing different site coordination and the layered structure

Normalized scale factor

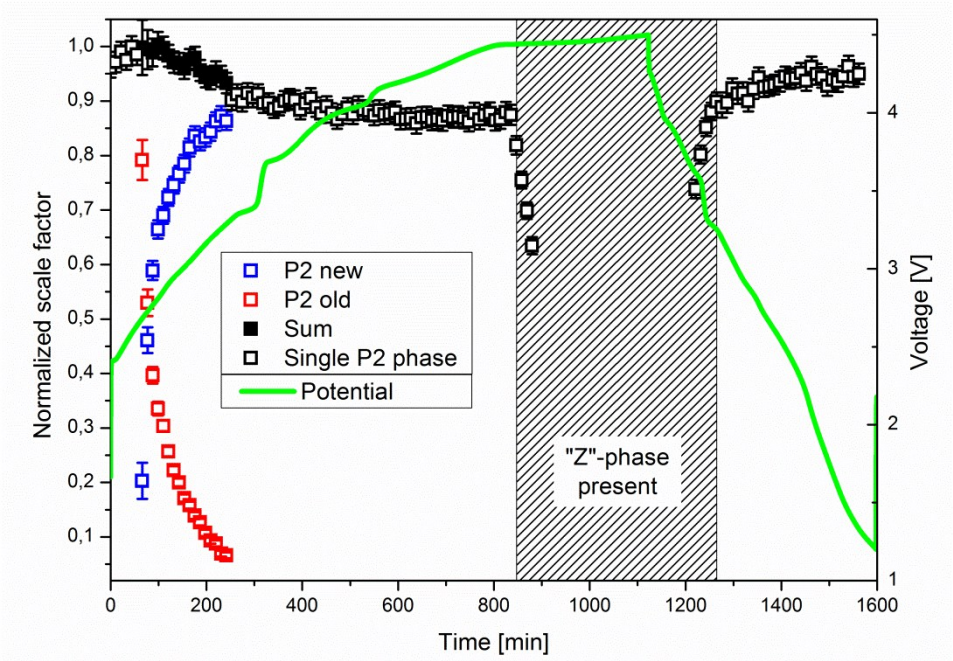

Figure S2. Normalized scale factor for P2 phases as a function of time

High potential phase transformation

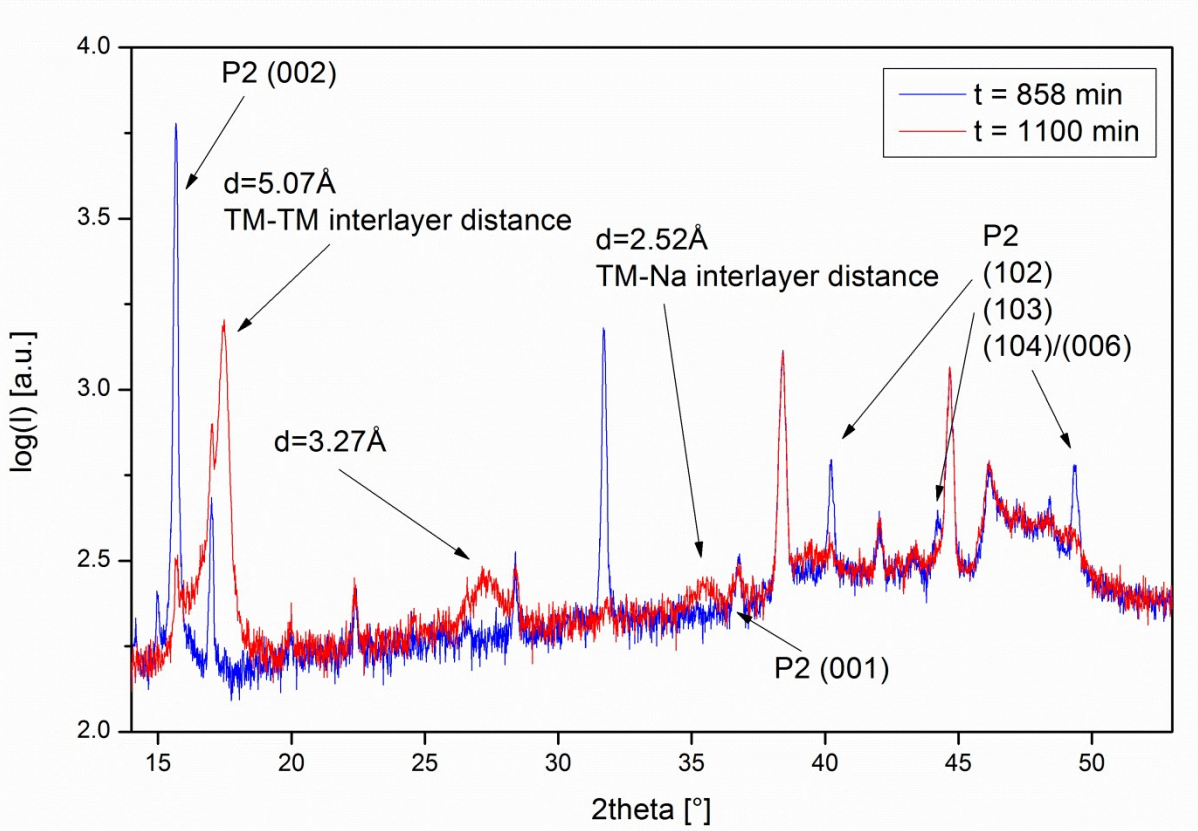

Figure S3. PXRD patterns at t = 858 min and t = 1100 min showing the difference between the patterns for P2-NCMO and the "Z" phase

At 847 minutes the Bragg reflections from the P2-NCMO phases start to disappear and a new set of few and broad Bragg reflections appear instead (see Fig. 1 in the manuscript). The phase transformation is accompanied by a plateau close to 4.5 V in the cell voltage curve. The plateau is reversible upon further cycling, which indicates that the phase transformation is reversible. The new peaks arise from a new poorly crystalline phase, probably related to the previously reported high potential phases.[1-6] These high potential phases are often hard to characterize structurally because of poor crystallinity and often termed "Z", OP4 or disordered O2 phase. The formation mechanism probably involves gliding of the TM-sheets to form octahedral sodium sites when almost all sodium has been extracted from the structure. Because of different choices of gliding directions these phases always display a high degree of stacking faults. Even though at least two articles have reported a detailed structure for these high potential phases,[3, 5] it seems that the exact structure varies, and depends strongly on the exact composition of the original P2 material. The new phase appearing at high potential in this work is termed the "Z" phase since that name has appeared as a generic term for these phases in the literature.

Detailed analysis of the structure of the "Z" phase using Rietveld refinements is not possible due to poor crystallinity. Instead a few qualitative conclusions are drawn by analysing the Bragg reflection positions relative to the P2-NCMO just before the phase transformation. Figure S3 shows the in operando datasets collected at t = 858 min (just before the high potential phase transformation initiates) and t = 1100 min (end of charge where the "Z" phase is maximal). Firstly, after full charging to 4.5V the phase transformation is not fully completed since the (002) peak from the P2 phase is still visible. The incomplete phase transformation could be due to slight inhomogeneity in the state of charge due to the flexible aluminium current collector as will be commented on later. Secondly, the peak appearing at $2\theta \approx 17.5°$ ($d \approx 5.07$ Å) probably originates from the average interlayer distance between the transition metal oxide sheets (TM-sheets). The sudden drop in interlayer spacing compared to the P2-NCMO phase indicates a change in the coordination environment for the sodium atoms, which may change from a prismatic site to an octahedral site. This happens as a result of gliding of the TM-sheets giving a closer packing of the oxide ions and therefore a drop in the TM-sheet interlayer distance. As described by Lu et al. for P2-$Na_xNi_{0.3}Mn_{0.7}O_2$ there are two possible glide directions giving a change in oxygen stacking as ABBA→ABCB or ABBA→ABAC.[7] Because the glide direction is chosen at random, a high degree of stacking faults is induced in the "Z" phase. This destroys the long range correlation along (10l) directions, which is evident by the smearing out of the (10l)

peaks going from the P2 phase to the "Z" phase. The glide mechanism is also supported by the fact that the (100) reflection doesn't change during the phase transformation indicating that the structure of single TM-sheets is preserved. A weak peak appearing at 2θ≈35.6° (d≈2.52 Å) or approximately half the TM-sheet interlayer distance indicates that there is some electron density half way in between the TM-sheets. The electron density is most probably due to residual sodium ions sitting in the octahedral site meaning the "Z" phase is not sodium free. Finally, the peak appearing at 2θ≈27.3° (d≈3.27 Å) could arise from electron density from transition metal atoms that move out of their octahedral sites in the TM-sheets into a tetrahedral site right above/below them as would be consistent with the structure reported by Talaie et al.[3] Note that the peak at d≈3.27 Å has not been reported in diffractograms of the "Z" phase before indicating that the detailed structure of this "Z" phase is somewhat different that previously reported.

Experimental section

Synthesis

$Na_xCo_{0.7}Mn_{0.3}O_2$, hereafter termed NCMO, was prepared using a two-step synthesis method as reported in detail elsewhere.[8] The first step was a co-precipitation of $Co_{0.7}Mn_{0.3}C_2O_4{\cdot}2H_2O$ using a 0.25 M transition metal sulphate solution (Co^{2+}:Mn^{2+}=7:3) and 0.25 M $Na_2C_2O_4$ solution. The pink powdered product was washed and dried and used as a precursor in the second step of the synthesis. The second step was a high temperature solid state reaction. The oxalate precursor was thoroughly mixed with Na_2CO_3 in a mortar to give the atomic ratio $Na/Co_{0.7}Mn_{0.3}$=1.05 (5% excess of sodium was used to compensate for sodium evaporation in the high temperature synthesis). The powdered mixture was pressed into a pellet at room temperature and calcined in a muffle furnace at 900°C for 12 hours followed by a slow cooling. At 300°C the product was moved into an argon filled glove box and crushed into powder using a mortar. Samples from 4 different synthesis batches were used in the analysis for this article. All of the samples crystallized in the P2 phase (only containing very minor amounts of unknown impurities), and they were all refined to have the same crystal structure. Some differences in amorphous material content were observed (quantified by measured specific capacity in the 4.1-4.4 V plateau), probably due to different degrees of reaction because of the different batch sizes.

Characterization

NCMO was characterized for elemental composition, morphology and crystalline structure. Elemental analysis was performed using inductively coupled plasma optical emission spectroscopy (ICP-EOS) using a SPECTRO ARCOS instrument from AMETEK. High resolution transmission electron microscopy coupled with energy dispersive spectroscopy (HRTEM-EDS) was used to investigate morphology, homogeneity and elemental distribution of the samples. HRTEM-EDS was performed on a TALOS F200A with a TWIN lens system, X-FEG electron source, Ceta 16M Camera and a Super-X EDS Detector. Spatially resolved elemental analysis, with a spatial resolution better than 2 nm, was obtained using the same TALOS microscope in STEM mode. Exposure times of 5 minutes were used to create elemental distribution maps with satisfactory counting statistics, while minimizing potential problems such as beam damage and specimen drift. STEM pictures were obtained using a High Angle Annular Dark Field detector (HAADF). The crystal structure, hereafter termed P2-NCMO, was characterized using high resolution powder X-ray diffraction (PXRD) collected at beamline BL44B2, Spring8, Japan.[9] Samples were packed in 0.3 mm glass capillaries and spun during data collection in Debye-Scherrer geometry. A 24.8 keV beam was utilized giving a typical Q range of 0.8-15.6 $Å^{-1}$.

Rietveld refinements of pristine material

The PXRD data were analysed using Rietveld refinements[10] implemented in the computer program FullProf.[11] The PXRD pattern of P2-NCMO can be fitted to the ideal hexagonal P2 structure indicating successful synthesis of the desired crystalline phase, see Figure S4. Due to the very high flux during the synchrotron PXRD collection, minor impurities were detected, which would not be observed by conventional PXRD. The minute impurities are only seen when zooming into the background area, see Figure S5. One of the impurity phases is quartz, used in cleaning the mortar, but the other phases are unknown. Due to the very low amount of the impurity phases they are not included in the Rietveld analysis. The results of the Rietveld refinements are presented in Table S2. Restraining the sodium atoms to the high symmetry positions (2b for Na_f and 2d for Na_e) during Rietveld refinements gave unphysically large atomic displacement parameters (ADP, B_{iso}); this has been shown in many structural studies of the P2 structure.[4, 12, 13] Physically reasonable ADPs could be obtained either by splitting the sites into a lower symmetry 6h site or refining anisotropic ADPs.[3, 14-17] It was found that the best fit to the data was obtained by refining anisotropic ADPs for all metal atoms, but keeping the positions in high symmetry sites. The refined thermal ellipsoids for the sodium ions take on the form of a thin disc perpendicular to the *c*-axis. This relatively large thermal motion in the a/b-plane probably related to the diffusion of the sodium ions during battery cycling. The refined occupancies for the Na_f and Na_e sites are 0.22(1) and 0.39(1), respectively, giving a total of 0.61(1) sodium ions per formula unit in the crystalline phase. This is lower than the sodium content determined by ICP-

OES, indicating that a part of the sodium in the material is not incorporated into the crystalline structure, and thus the presence of a sodium rich amorphous phase. Higher occupancy in the Na_e site is expected since it is thermodynamically more stable than the Na_f site.[18-24] This is due to lower electrostatic repulsion between the transition metal atom and the sodium atom because of longer interatomic distance, ~2.8 Å and ~3.2 Å for TM to Na_f and Na_e respectively.

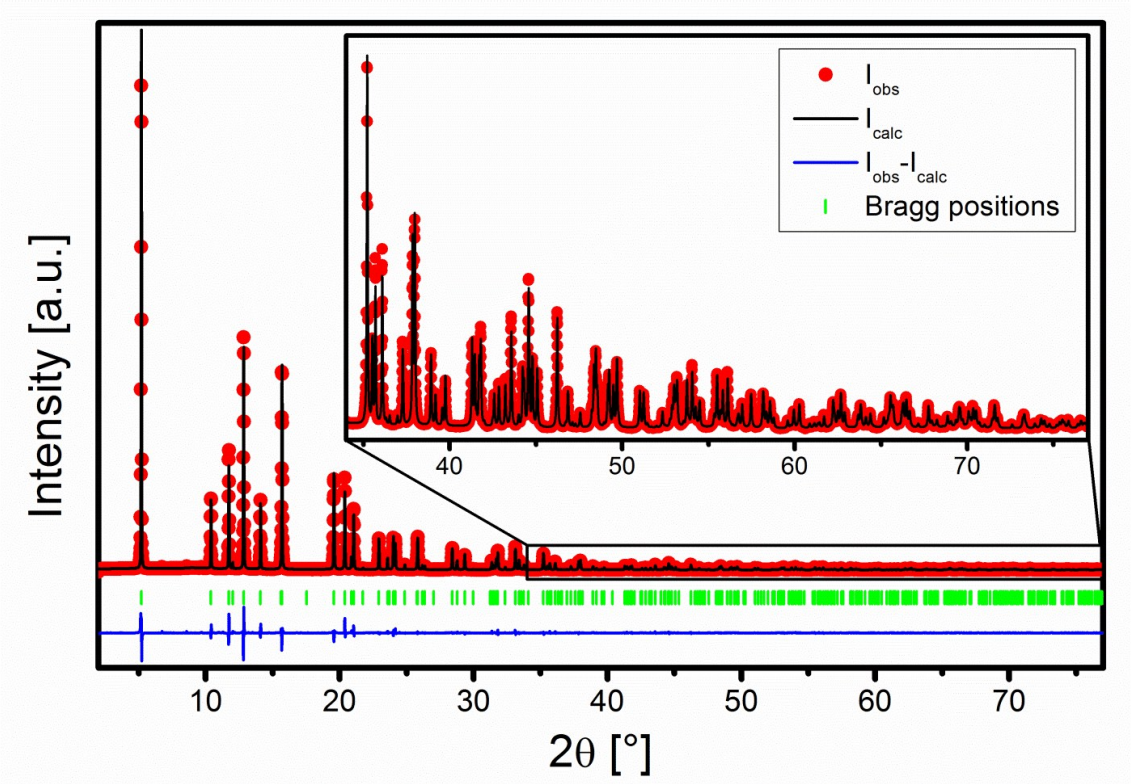

Figure S4. Rietveld refinement fit

Table S2. Results of Rietveld refinements.

Space Group	$P6_3/mmc$						
# of data points	7450						
# of background points	28						
Total # of parameters	46						
R_{wp}	11.8						
R_F	2.63						
Unit cell a=b (Å)	2.82814(1)						
Unit cell c (Å)	11.04804(5)						
Site	x	Y	z	Occupancy (*ICP/**fixed)	β_{11} (*B_{iso})	β_{33}	β_{12}
Na_f	0	0	¼	0.22(1)	0.11148(1346)	0.00049(43)	0.05574(673)
Na_e	⅓	⅔	¾	0.39(1)	0.14965(1082)	0.00123(39)	0.07482(541)
Co/Mn	0	0	½	*0.6943(6)/0.3057(6)	0.00833(42)	0.00109(3)	0.00417(21)
O	⅓	⅔	0.09061(12)	**2	*0.422(20)		

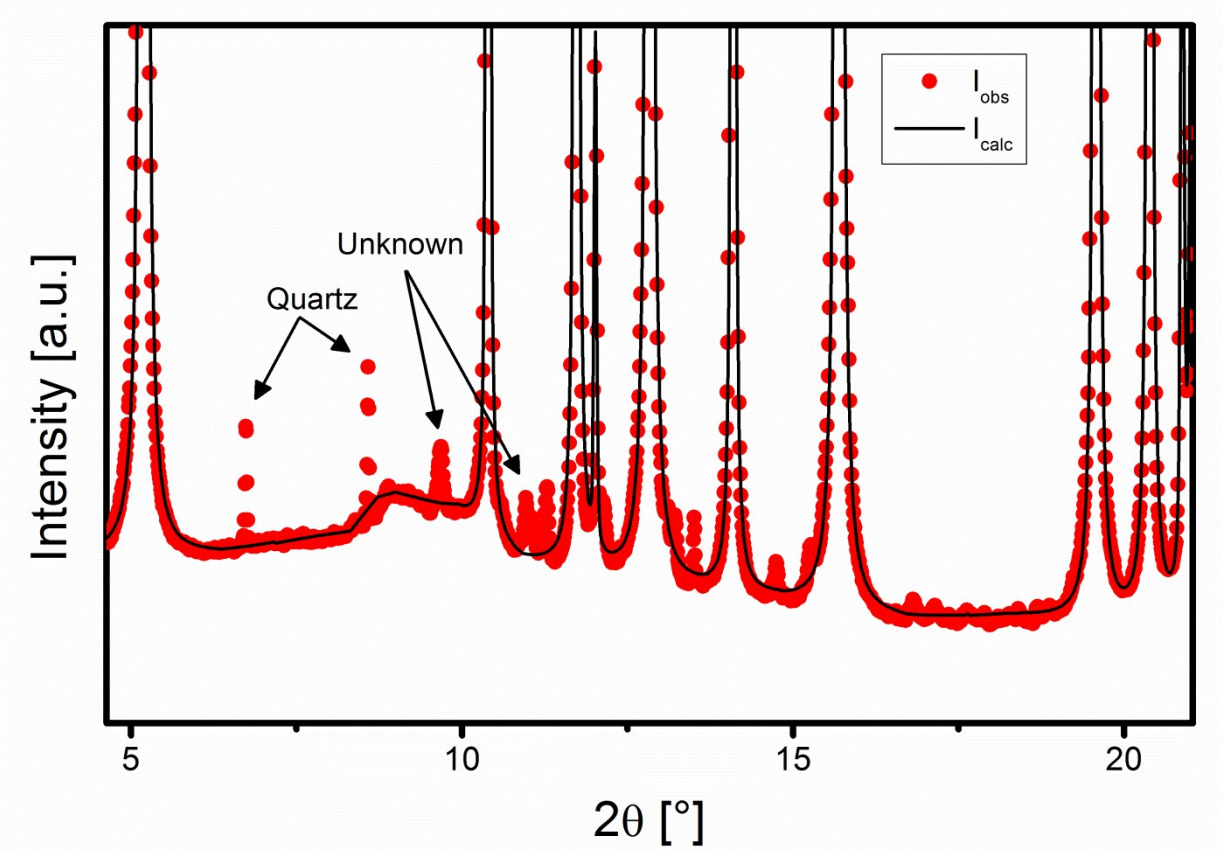

Figure S5. Impurities detected in PXRD

In operando data collection

Electrodes were prepared by coating a N-Methyl-2-pyrrolidone (NMP) slurry consisting of 80 wt% NCMO, 10% acetylene black and 10% polyvinylidene fluoride (PVDF) binder (on dry basis) onto a 15 µm thick aluminium foil from MTI corporation. Circular electrodes with a diameter of 15 mm were punched out giving an active material mass loading of ~3-4 mg. These electrodes were used as cathodes in half cell assemblies using sodium metal as the counter electrode, 1 M $NaClO_4$ in propylene carbonate (PC) (with 2% by weight fluorinated ethylene carbonate (FEC) as additive) as electrolyte and porous glass fibre (Whatman GF/D) as separator. The half-cell was assembled in an *in operando* cell, specially designed to measure PXRD data of sodium and lithium ion electrode materials during cycling using an in-house diffractometer. The *in operando* cell has been described in detail elsewhere.[25] The *in operando* cell is suitable for studying both bulk and nano materials although diffused scattering from nano materials makes data analysis of them more challenging, A few limitation in the design of the *in operando* cell should be kept in mind. The half-cell stack is pressed together by plastic screws pressing on a stainless steel ring with a 10 mm opening to allow X-rays to reach the electrode material. This limits the applied pressure, especially compared with conventional coin cells. This effect is minimized by charging the half cell at a low rate and potential curves obtained in the *in operando* cell have been shown to be almost identical to potential curves from coin cells.[25] There is non-uniform pressure due to flexible aluminium foil current collector, and this has been shown to affect how uniform the extent of the electrochemical reaction is.[26] This effect is minimized by charging slowly and by probing a relatively large volume of the electrode (ø = 10 mm opening on an ø = 15 mm electrode). A systematic error is present in the relative PXRD intensities due to 2θ dependent attenuation of the primary and diffracted beam when it passes through the current collector. This means that information extracted from intensities (such as occupancies) is only relative between datasets of the same *in operando* run, see discussions about sodium site occupancies below.

In operando measurements were performed for the first charge and discharge of the NCMO electrode with cut-off voltages of 4.5-1.2 V. Cycling was performed under constant current conditions at 0.05 mA (~10 mA/g). PXRD patterns were collected on Rigaku Smart-Lab diffractometer (with a rotating Cu anode at 140 mA and 40 kV giving mixed Cu $K\alpha_1$ and $K\alpha_2$ radiation) using parallel beam geometry in reflection mode (θ/2θ scan). The angular range was 2θ = 14-52° but the region with 2θ = 45.5-49.0° was excluded from the Rietveld refinements because it showed a large diffuse diffraction

hump from the graphite dome. Each scan took approximately 11 minutes to be collected. Charging to 4.5 V took ~1120min (~C/19) giving a time resolution of Δt/t≈0.01. The discharge capacity was lower, resulting in a discharge time of ~480 min (~C/8), giving a Δt/t≈0.02. The relatively low coulombic efficiency can partly been explained by the amorphous phase reacting irreversibly in the potential range from ~4.1-4.4 V. Further explanation might include electrolyte decomposition[27] and/or solid electrolyte interface[28] formation during first charging.

In operando data analysis

The time resolved *in operando* PXRD data was analysed by sequential Rietveld refinements in Fullprof.[11] The starting structural model included the P2-NCMO phase as refined from the pristine material and a cubic aluminium phase (Space group: $Fm\bar{3}m$). Peak broadening due to the instrument was accounted for by instrumental resolution file (IRF) refined from a LaB_6 standard in the same instrumental configurations. The refined sample and/or instrumental parameters in the sequential refinements were zero point displacement and the background, modelled using a linear interpolation between 12 background points hand-picked to fit features in the background but not affecting the Bragg reflections. In the first *in operando* PXRD dataset (t = 0 min) the scale factor, unit cell, peak profile (two pseudo-Voigt parameters, U and X) and preferred orientation were refined for the aluminium phase to give an arbitrary fit to the two observed Bragg reflections. For the sequential refinements all parameters for the aluminium phase except scale factor were fixed. The refined aluminium scale factor was used to normalize the scale of the P2-NCMO phase assuming that the aluminium phase stayed constant for the whole *in operando* experiment. For the t = 0 min dataset the P2-NCMO phase was refined keeping all structural and microstructural parameters fixed except for scale factor, unit cell parameters, peak profile (one pseudo-Voigt parameters, U), preferred orientation and occupancies for Na_e and Na_f. Due to the platelet morphology of the crystallites[8] the P2-NCMO phase showed a high degree of preferred orientation after being coated on the electrode. Because of this and unknown 2θ dependent attenuation of the diffracted x-ray from the aluminium current collector, systematic errors in measured relative intensities were observed. The preferred orientation was modelled in the t = 0 min dataset using a modified March's function,[29] but kept fixed during sequential refinements. This is a reasonable assumption since the crystallites cannot move in the electrode coating. All other structural parameters that were refined for P2-NCMO in the t = 0 min dataset were refined sequentially.

Notes about sequentially refined sodium occupancies

Due to the previously mentioned systematic error to the relative intensities, unphysically large occupancies were refined for the two sodium sites in the *in operando* data (note that the only sequentially refined parameters affecting the relative intensities are the occupancies for the two sodium sites). Because the systematic error is constant for all datasets the relative changes in refined occupancies for Na_e and Na_f are reliable even though the absolute value is in error. Thus by assuming that the P2-NCMO material measured at t = 0 min has the same sodium site occupancy as the pristine material, the relative changes in occupancies can be converted into an absolute scale. This is done by calculating a simple additive correction factor to convert the wrong occupancy into the correct one for the t = 0 min dataset and then adding it to all datasets in the in operando run as follows:

$$x(Na_f)(t=0) + C(Na_f) = x(Na_f)(pristine)$$

$$\Rightarrow 0.4798 + C(Na_f) = 0.2236$$

$$\Rightarrow C(Na_f) = -0.2562$$

$$x(Na_e)(t=0) + C(Na_e) = x(Na_e)(pristine)$$

$$0.9224 + C(Na_e) = 0.3919$$

$$\Rightarrow C(Na_e) = -0.5305$$

In the *in operando* data sets there are two P2 phases with different *c*-axis values present (t = 66-242 min), but it is not possible to reliable refine occupancies for both P2 phases simultaneously. This is because of excessive peak overlap, which makes it impossible to assign a relative intensity to each phase. To compensate for this the sequential refinements

were constrained to only refine occupancies for one of the P2 phases, while keeping the other phase fixed. Therefore, the refined occupancies for each individual phase are probably slightly wrong but the weighted average is reliable and corresponds to the average occupancy of both phases. Refinements have also been carried out using only a single P2 phase and the Na occupancies do not change significantly (but the residual factors degrade since there are two P2 phases present).

Elemental composition

Elemental ratios for sodium, cobalt and manganese are presented in Table S1.

Table S1. ICP-OES results and calculated atomic ratios for sodium, cobalt and manganese.

Element	ICP-OES concentration [mg/L]	Atomic ratio
Sodium	0.815(9)	0.808(9)
Cobalt	1.796(1)	0.6943(6)
Manganese	0.737(2)	0.3057(6)

High Resolution Transmission Electron Microscopy coupled with Energy Dispersive Spectroscopy

HRTEM revealed two types of particles present in NCMO. The first type shows crystallite facets and lattice fringes; see Figure S6a, b. These particles are therefore most probably the crystalline P2-NCMO detected by PXRD. The second particle type has a fluffy morphology with little indication of crystallinity, Figure S6c. The presence of the fluffy particles reveals that the NCMO material contains an amorphous phase as was indirectly indicated by elemental analysis versus refined sodium loading. The fact that the amorphous material appears in separate particles from the crystalline particles suggest the amorphous material is not homogeneously distributed on the nano scale. The EDS pictures, presented in Figure S7, show that the P2-NCMO phase contains sodium, cobalt, manganese and oxygen confirming that all the expected elements are included in the P2-NCMO phase. The fluffy particle shows a very limited inclusion of cobalt while sodium, manganese and oxygen are definitely present. This supports the conclusion drawn from the elemental analysis that the amorphous phase is sodium rich. As discussed in the article this amorphous phase is probably responsible for the electrochemical activity in the voltage range 4.1-4-4 V.

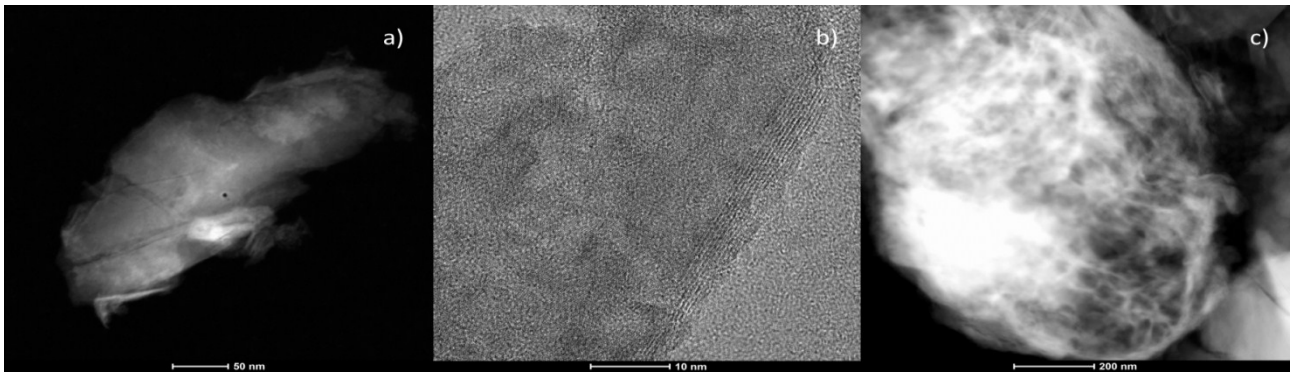

Figure S6. HRTEM pictures of a) crystalline P2-NCMO particle, b) lattice fringes and c) fluffy particle

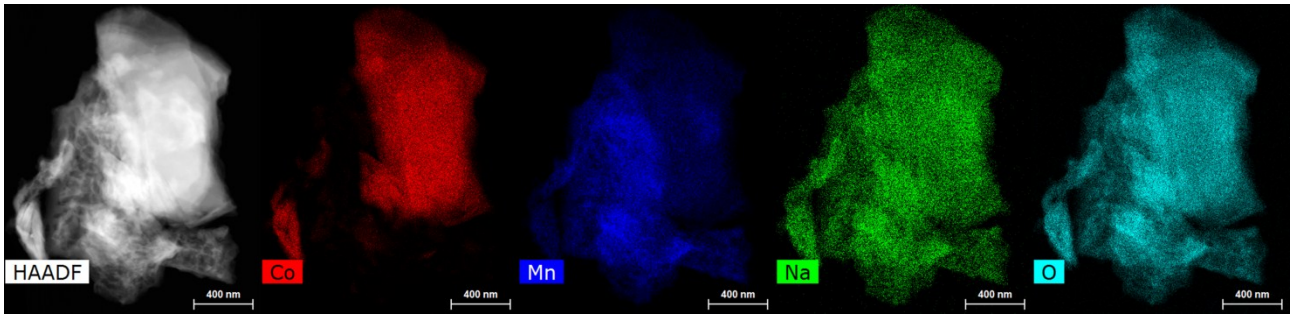

Figure S7. STEM-EDS pictures showing the distribution of elements (cobalt=red, manganese=dark blue, sodium=green, oxygen=light blue) of a particle consisting of a crystalline and a fluffy part. The crystalline part has a homogenous distribution of all elements indicating the P2 structure contains all the expected elements. The fluffy part is obviously poorer in cobalt compared to the other elements.

References

1. B. Mortemard de Boisse, D. Carlier, M. Guignard, L. Bourgeois and C. Delmas, *Inorg. Chem.*, 2014, **53**, 11197-11205.
2. E. Gonzalo, M. H. Han, J. M. Lopez del Amo, B. Acebedo, M. Casas-Cabanas and T. Rojo, *J. Mater. Chem. A*, 2014, **2**, 18523-18530.
3. E. Talaie, V. Duffort, H. L. Smith, B. Fultz and L. F. Nazar, *Energy Environ. Sci.*, 2015, **8**, 2512-2523.
4. L. Liu, X. Li, S.-H. Bo, Y. Wang, H. Chen, N. Twu, D. Wu and G. Ceder, *Adv. Energy Mater.*, 2015, **5**, 1500944.
5. N. Yabuuchi, M. Kajiyama, J. Iwatate, H. Nishikawa, S. Hitomi, R. Okuyama, R. Usui, Y. Yamada and S. Komaba, *Nat. Mater.*, 2012, **11**, 512-517.
6. S. Kumakura, Y. Tahara, K. Kubota, K. Chihara and S. Komaba, *Angew. Chem., Int. Ed.*, 2016, **55**, 12760-12763.
7. Z. Lu and J. R. Dahn, *J. Electrochem. Soc.*, 2001, **148**, A1225-A1229.
8. Y. Shen, S. Birgisson and B. B. Iversen, *J. Mater. Chem. A*, 2016, **4**, 12281-12288.
9. E. Nishibori, M. Takata, K. Kato, M. Sakata, Y. Kubota, S. Aoyagi, Y. Kuroiwa, M. Yamakata and N. Ikeda, *J. Phys. Chem. Solids*, 2001, **62**, 2095-2098.
10. H. Rietveld, *J. Appl. Crystallogr.*, 1969, **2**, 65-71.
11. J. Rodríguez-Carvajal, *Phys. B*, 1993, **192**, 55-69.
12. D. Carlier, J. H. Cheng, R. Berthelot, M. Guignard, M. Yoncheva, R. Stoyanova, B. J. Hwang and C. Delmas, *Dalton Trans.*, 2011, **40**, 9306-9312.
13. J. Xu, S.-L. Chou, J.-L. Wang, H.-K. Liu and S.-X. Dou, *ChemElectroChem*, 2014, **1**, 371-374.
14. N. Yabuuchi, R. Hara, M. Kajiyama, K. Kubota, T. Ishigaki, A. Hoshikawa and S. Komaba, *Adv. Energy Mater.*, 2014, **4**, 1301453.
15. V. Duffort, E. Talaie, R. Black and L. F. Nazar, *Chem. Mater.*, 2015, **27**, 2515-2524.
16. Y. Ono, N. Kato, Y. Ishii, Y. Miyazaki and T. Kajitani, *J. Jpn. Soc. Powder Powder Metall.*, 2003, **50**, 469-474.
17. Y. Takahashi, J. Akimoto, N. Kijima and Y. Gotoh, *Solid State Ionics*, 2004, **172**, 505-508.
18. G. J. Shu, A. Prodi, S. Y. Chu, Y. S. Lee, H. S. Sheu and F. C. Chou, *Phys. Rev. B*, 2007, **76**, 184115.
19. R. Berthelot, D. Carlier and C. Delmas, *Nat. Mater.*, 2011, **10**, 74-80.
20. Q. Huang, M. L. Foo, J. W. Lynn, H. W. Zandbergen, G. Lawes, W. Yayu, B. H. Toby, A. P. Ramirez, N. P. Ong and R. J. Cava, *J. Phys.: Condens. Matter*, 2004, **16**, 5803-5814.
21. P. Zhang, R. B. Capaz, M. L. Cohen and S. G. Louie, *Phys. Rev. B*, 2005, **71**, 153102.
22. Y. Hinuma, Y. S. Meng and G. Ceder, *Phys. Rev. B*, 2008, **77**, 224111.
23. Y. S. Meng, Y. Hinuma and G. Ceder, *J. Chem. Phys.*, 2008, **128**, 104708.
24. D. H. Lee, J. Xu and Y. S. Meng, *Phys. Chem. Chem. Phys.*, 2013, **15**, 3304-3312.
25. Y. Shen, E. E. Pedersen, M. Christensen and B. B. Iversen, *Rev. Sci. Instrum.*, 2014, **85**, 104103.
26. O. J. Borkiewicz, K. M. Wiaderek, P. J. Chupas and K. W. Chapman, *J. Phys. Chem. Lett.*, 2015, **6**, 2081-2085.
27. K. Kubota and S. Komaba, *J. Electrochem. Soc.*, 2015, **162**, A2538-A2550.
28. A. Ponrouch, D. Monti, A. Boschin, B. Steen, P. Johansson and M. R. Palacin, *J. Mater. Chem. A*, 2015, **3**, 22-42.
29. W. Dollase, *J. Appl. Crystallogr.*, 1986, **19**, 267-272.